International Journal of Engineering Research and Science & Technology

IJERST

www.ijerst.org

ISSN : 2319-5991

Vol. 18 No. 3 (2022)

ijerst.editor@gmail.com
editor@ijerst.com

ISSN 2319-5991 www.ijerst.com
Vol. 18, No. 3, 2022

Research Paper

HEAT TRANSFER EFFECTS ON PERISTALTIC TRANSPORT OF PARTICLE-SUSPENDED COUPLE STRESS FLUIDS

T. Raghunatha Rao*
Department of Mathematics & Humanities, Kakatiya Institute of Technology & Science, Warangal, Affiliated to Kakatiya University, Warangal, Telangana, India.
**Email: tangedaraghunathrao@gmail.com*

Received: 06-07-2022 Accepted: 11-09-2022 Published: 18-09-2022

ABSTRACT

The peristaltic motion of a couple stress fluid permeated with suspended particles through a two-dimensional flexible channel under long wavelength approximation with heat transfer is studied. A perturbation method of solution is obtained in terms of wall slope parameter and closed form of expressions has been derived for axial velocity and transverse velocity in fluid phase and particle phase. The expression heat transfer has been computed numerically using mathematics software Mathematica. The graphical results have been presented to discuss the physical behaviour of various physical parameters on geometric parameter, Prandtl number and Couple stress parameter. The variation of heat transfer with Prandtl number shows that the heat transfer coefficient experiences a depreciation with Prandtl number the depreciation on the boundary at $y = 1$ is appreciably large.

Keywords: *Peristaltic motion, Couple stress fluid, suspended particles, Heat transfer.*

1. INTRODUCTION

The effects of heat transfer on peristaltic transport of particle-suspended couple stress fluids have been extensively studied across various research domains, including biomedical applications and microfluidic systems. Vidhya et al. (2015) analyzed the impact of thermal gradients on the MHD peristaltic flow of couple stress fluids and found that Grashof number and heat source parameters significantly influence pressure rise and friction forces, particularly in applications involving biological flows. Similarly, Prasad et al. (2017) investigated the role of nanoparticles in peristaltic transport, where Brownian motion and thermophoresis altered temperature profiles and particle distribution, emphasizing the enhancement of heat transfer in microfluidic devices. Bhatti et al. (2017) contributed significantly by examining the interaction between heat transfer and suspended particles in couple stress fluids, revealing that suspended particles modify the temperature distribution and flow characteristics, affecting heat exchange efficiency. Ramesh and Devakar (2015) explored MHD effects in peristaltic flows, highlighting the Hartmann number as a key factor in determining the thermal and fluid flow behavior, particularly in biofluid applications. Maiti and Misra (2012) provided foundational insights into the dynamics of couple stress fluids, showing how particle interactions influence both temperature gradients and flow characteristics in physiological contexts. Ellahi et al. (2018) further extended this work by incorporating the effects of magnetic fields and thermal gradients, demonstrating their combined influence on heat transport in peristaltic systems. The studies by Bhatti and Ellahi (2021) focused on nanoparticle-laden couple stress fluids, highlighting the crucial role of particle size and thermal conductivity in enhancing heat transfer efficiency in biomedical devices. Ahmed et al. (2016) contributed by studying the peristaltic motion of blood flow in a couple stress fluid model, showing how temperature changes affect the pulsatile flow in arterial models. Ghosh and Roy (2017) investigated fluid-particle interactions in microfluidic channels, noting that heat and mass transfer effects become more pronounced in confined spaces, leading to changes in particle distribution and flow resistance. Lastly, Raju et al. (2019) examined the thermal conductivity of suspended particle systems, showing that particle concentration plays a significant role in thermal regulation within peristaltic transport systems, thereby optimizing energy exchange and fluid efficiency in lab-on-a-chip technologies. These studies collectively emphasize the importance of integrating thermal dynamics with particle transport for improved fluid flow and heat transfer in applications ranging from drug delivery systems to biomedical flow diagnostics.

Significance of the work

In this work, to understanding the complex dynamics of peristaltic transport in couple stress fluids with suspended particles under heat transfer effects. By providing a detailed analysis of how key parameters, such as the Prandtl number and couple stress, influence flow behavior and heat transfer, this study enhances the design and optimization of microfluidic systems and biomedical applications. The findings offer valuable insights for applications in drug delivery, biofluid transport, and heat management in small-scale systems

2.Methodology

The methodology of this study involves deriving closed-form expressions for axial and transverse velocities in both the fluid and particle phases under the long wavelength approximation. A perturbation method is employed, considering the wall slope parameter to solve the peristaltic flow problem. Heat transfer effects are analyzed numerically using Mathematica, with results presented graphically to examine the influence of physical parameters such as the Prandtl number, couple stress parameter, and geometric parameters. The approach provides insights into the thermal behavior and flow characteristics of particle-suspended couple stress fluid.

3. FORMULATION OF THE PROBLEM

We consider a peristaltic flow of a dusty viscous incompressible couple stress fluid through a two-dimensional channel bounded by flexible walls.

The geometry of the flexible walls is represented by

$$y=\eta(x,t)=d+a\ \mathrm{Sin}\frac{2\pi}{\lambda}(x-ct) \tag{1}$$

Where'd' is the mean half width of the channel ' a ' is the amplitude of the peristaltic wave, ' c ' is the wave velocity, ' λ ' is the wave length and 'c' is the phase speed of the wave.

The equations governing the two-dimensional flow of a dusty viscous in compressible couple stress fluid in fluid phase are

$$\frac{\partial u}{\partial x}+\frac{\partial v}{\partial y}=0 \tag{2}$$

$$\rho\left(\frac{\partial u}{\partial t}+u\frac{\partial u}{\partial x}+v\frac{\partial u}{\partial y}\right)=-\frac{\partial p}{\partial x}+\mu\left(\frac{\partial^2 u}{\partial x^2}+\frac{\partial^2 u}{\partial y^2}\right)-\eta\left(\frac{\partial^4 u}{\partial x^4}+\frac{\partial^4 u}{\partial y^4}+2\frac{\partial^4 u}{\partial x^2\partial y^2}\right)-K\,N(u^p-u) \tag{3}$$

$$\rho\left(\frac{\partial v}{\partial t}+u\frac{\partial v}{\partial x}+v\frac{\partial v}{\partial y}\right)=-\frac{\partial p}{\partial y}+\mu\left(\frac{\partial^2 v}{\partial x^2}+\frac{\partial^2 v}{\partial y^2}\right)-\eta\left(\frac{\partial^4 v}{\partial x^4}+\frac{\partial^4 v}{\partial y^4}+2\frac{\partial^4 v}{\partial x^2\partial y^2}\right)-K\,N(v^p-v) \tag{4}$$

Equation of energy

$$\rho C_p\left(\frac{\partial T}{\partial t}+u\frac{\partial T}{\partial x}+v\frac{\partial T}{\partial y}\right)=k\left(\frac{\partial^2 T}{\partial x^2}+\frac{\partial^2 T}{\partial y^2}\right)+\rho\upsilon\left(\frac{\partial u}{\partial y}+\frac{\partial v}{\partial x}\right)^2+\frac{N m C_s}{\tau_p}(T^p-T) \tag{5}$$

The equations governing the two-dimensional flow of a dusty viscous in compressible couple stress fluid in particle phase are

$$\frac{\partial N}{\partial x}+N\left(\frac{\partial u^p}{\partial x}+\frac{\partial v^p}{\partial y}\right)=0 \tag{6}$$

$$\frac{\partial u^p}{\partial t}+u^p\frac{\partial u^p}{\partial x}+v^p\frac{\partial u^p}{\partial y}=\frac{k}{m}(u-u^p) \tag{7}$$

$$\frac{\partial v^p}{\partial t}+u^p\frac{\partial v^p}{\partial x}+v^p\frac{\partial v^p}{\partial y}=\frac{k}{m}(v-v^p) \tag{8}$$

Equation of energy

$$\frac{\partial T^p}{\partial t}+u^p\frac{\partial T^p}{\partial x}+v^p\frac{\partial T^p}{\partial y}=\left(\frac{T-T^p}{\tau_p}\right) \tag{9}$$

Where 'p' is the fluid pressure, 'ρ' is the density of the fluid, μ is the coefficient of viscosity, m is the mass of the dust particle, Nis the number density of the particles, k is the stokes resistance coefficient. The particles are assumed to be uniform in size and uniformly distributed in the fluid so that N remains constant.

The relative boundary conditions are

$$u=0 \quad \text{at} \quad y=\pm\eta \tag{10}$$

$$\frac{\partial^2 u}{\partial y^2}=0 \quad \text{at} \quad y=\pm\eta \tag{11}$$

$$v=0 \quad \text{at} \quad y=0 \tag{12}$$

$$T=T_0 \quad \text{at}\ y=-\eta\ , \quad T=T_1 \quad \text{at}\ y=\eta \tag{13}$$

Introducing a wave frame (x, y) moving with velocity c away from the fixed frame (X,Y) by the transformation

$$x=X-c\,t,\ y=Y$$

We introduced the non-dimensional variables as

$$x'=\frac{x}{\lambda},\ y'=\frac{y}{d},\ u'=\frac{u-c}{c},\ u^{p'}=\frac{u^p-c}{c},\ v'=\frac{v}{c\,\delta},\ v^{p'}=\frac{v^p}{c\,\delta}\ t'=\frac{c\,t}{\lambda},\ \eta'=\frac{\eta}{d},\ p'=\frac{p\,d^2}{\mu\,c\,\lambda},\ \theta=\frac{T-T_0}{T_1-T_0},$$

$$\theta^*=\frac{T^p-T_0}{T_1-T_0} \tag{14}$$

Substituting (14) in (3), (4), (5) and (7), (8) and (9) these equations reduce to (after dropping primes)

$$R\,\delta\left(\frac{\partial u}{\partial t}+u\frac{\partial u}{\partial x}+v\frac{\partial u}{\partial y}\right)=-\frac{\partial p}{\partial x}+\left(\frac{\partial^2 u}{\partial y^2}+\delta^2\frac{\partial^2 u}{\partial x^2}\right)$$
$$-S\left(\frac{\partial^4 u}{\partial y^4}+\delta^4\frac{\partial^4 u}{\partial x^4}+2\,\delta^2\frac{\partial^4 u}{\partial x^2\partial y^2}\right)+\frac{R\alpha}{\zeta}(u^p-u) \tag{15}$$

$$R\delta^3\left(\frac{\partial v}{\partial t}+u\frac{\partial v}{\partial x}+v\frac{\partial v}{\partial y}\right)=-\frac{\partial p}{\partial y}+\delta^2\left(\frac{\partial^2 v}{\partial y^2}+\delta^2\frac{\partial^2 v}{\partial x^2}\right)$$
$$-S\,\delta^2\left(\frac{\partial^4 v}{\partial y^4}+\delta^4\frac{\partial^4 v}{\partial x^4}+2\,\delta^2\frac{\partial^4 v}{\partial x^2\partial y^2}\right)-\frac{R\alpha}{\zeta}\delta^2(v^p-v) \tag{16}$$

$$\delta\left(\frac{\partial\theta}{\partial t}+u\frac{\partial\theta}{\partial x}+v\frac{\partial\theta}{\partial y}\right)=\frac{1}{R\,p_r}\left(\frac{\partial^2\theta}{\partial y^2}+\delta^2\frac{\partial^2\theta}{\partial x^2}\right)+\frac{E}{R}\left(\frac{\partial u}{\partial y}+\frac{\partial v}{\partial x}\right)^2-\frac{\alpha\,\nu}{\zeta}(\theta^P-\theta) \tag{17}$$

$$\frac{\partial N}{\partial t}+N\left(\frac{\partial u^p}{\partial x}+\frac{\partial v^p}{\partial y}\right)=0 \tag{18}$$

$$\delta\left(\frac{\partial u^p}{\partial x}+u^p\frac{\partial u^p}{\partial y}+v^p\frac{\partial u^p}{\partial y}\right)=\frac{1}{\zeta}(u-u^p) \tag{19}$$

$$\delta\left(\frac{\partial v^p}{\partial x}+u^p\frac{\partial v^p}{\partial y}+v^p\frac{\partial v^p}{\partial y}\right)=\frac{1}{\zeta}(v-v^p) \tag{20}$$

$$\delta\left(\frac{\partial \theta^p}{\partial x}+u^p\frac{\partial \theta^p}{\partial y}+v^p\frac{\partial \theta^p}{\partial y}\right)=\frac{1}{\zeta}(\theta-\theta^p) \tag{21}$$

The boundary conditions are

$$u=-1 \quad \text{at} \quad y=\pm\eta \tag{22}$$

$$\frac{\partial^2 u}{\partial y^2}=0 \quad \text{at} \quad y=\pm\eta \tag{23}$$

$$\theta=0 \quad \text{at} \quad y=-\eta, \qquad \theta=1 \quad \text{at} \quad y=\eta \tag{24}$$

Where

$\varepsilon=\frac{a}{d}$, $\delta=\frac{d}{\lambda}$ are geometric parameters, $R=\frac{cd}{\nu}$ is the Reynolds number

$P_r=\frac{\rho C_p \nu}{k_1}$ is the Prandtl number, $S=\frac{\eta}{\mu d^2}$ is the Couple stress parameter

$\gamma=\frac{C_s}{C_p}$ is the Ratio of specific heats, $\zeta=\frac{c\,m}{k\,d}$ is the Relaxation time

$\alpha=\frac{N\,m}{\rho}$ is the Dust concentration parameter, $E=\frac{c^2}{C_p(T_1-T_0)}$ is the Eckert number

4. METHOD OF SOLUTION

We seek perturbation solution for the following functions in terms of small parameter δ as follows:

$$u=u_0+\delta u_1+\delta^2 u_2+...... \tag{25}$$

$$u^p=u_0{}^p+\delta u_1{}^p+\delta^2 u_2{}^p+...... \tag{26}$$

$$\theta=\theta_0+\delta\theta_1+\delta^2\theta_2+...... \tag{27}$$

$$\theta^p=\theta_0{}^p+\delta\theta_1{}^p+\delta^2\theta_2{}^p+...... \tag{28}$$

Solving the equations (15 -21) subject to the conditions (22-24), we get

$$u_0=u_0{}^p=G_1+G_2\,\mathrm{Cosh}\,\beta y+G_3 y^2 \tag{29}$$

$$\theta_0=\theta_0{}^p=\frac{L_6}{12}y^4+\frac{L_7}{\beta^2}y\,\mathrm{Sinh}\,[\beta y]-\frac{2L_7}{\beta^3}\mathrm{Cosh}[\beta y]+\frac{L_8}{4\beta}\mathrm{Sinh}\,[2\beta y]-\frac{L_8}{2}y+B_9 y+B_{10} \tag{30}$$

$$u_1 = B_5 + B_7 \text{ Cosh } \beta y + h_1 y \text{ Sinh } \beta y + h_2 y^3 \text{ Sinh } \beta y + h_3 y^2 \text{Cosh } \beta y - h_4 y^2 - h_5 y^4 \tag{31}$$

$$u_1^p = h_6 \text{Cosh } \beta y + h_7 y \text{ Sinh } \beta y + h_8 y^2 \text{Cosh } \beta y + h_2 y^3 \text{ Sinh } \beta y - h_9 y^2 - h_5 y^4 - h_{10} \text{Cosh}(2 \beta y) + h_{11} \tag{32}$$

$$\begin{aligned}\theta_1 = {} & R_1 \text{ Cosh } \beta y + R_9 \text{ Sinh } \beta y + R_8 \text{ Cosh } 2\beta y + R_3 \text{ Sinh } 2\beta y + R_{10} \text{ Sinh } 3\beta y + R_{11} \text{ y Cosh } \beta y \\ & + R_2 \text{ ySinh } \beta y - R_{16} \text{ yCosh } 2\beta y + R_7 \text{ y Sinh } 2\beta y + R_6 y^2 \text{Cosh } \beta y + R_{19} y^2 \text{Sinh } \beta y + \\ & R_{25} y^2 \text{Cosh } 2\beta y + R_{15} y^2 \text{Sinh } 2\beta y + R_{21} y^3 \text{Cosh } \beta y + R_5 y^3 \text{Sinh } \beta y + R_{27} y^3 \text{Sinh } 2\beta y \\ & + R_4 y^4 \text{Cosh } \beta y - R_{23} y^4 \text{Sinh } \beta y + R_{26} y^4 \text{Cosh } 2\beta y + R_{22} y^5 \text{Cosh } \beta y + R_{20} y^5 \text{Sinh}\beta y + \\ & R_{28} + R_{24} y^6 \text{Cosh } \beta y + R_{28} y^5 \text{Sinh } 2\beta y + R_{29} y^6 \text{Cosh } 2\beta y - R_{12} y^6 + R_{17} y^5 + R_{18} y^4 \\ & + R_{13} y^3 + R_{14} y^2 + R_{30} y + R_{31}\end{aligned} \tag{33}$$

$$\begin{aligned}\theta_1^p = {} & R_{32} \text{Cosh } \beta y + R_{33} \text{Sinh } \beta y + R_{34} \text{Cosh } 2\beta y + R_{35} \text{ Sinh } 2\beta y + R_{10} \text{ Sinh } 3\beta y + \\ & R_{36} \text{ y Cosh } \beta y + R_{37} \text{ySinh } \beta y + R_{38} \text{yCosh } 2\beta y + R_{39} \text{y Sinh } 2\beta y + R_{40} y^2 \text{Cosh } \beta y + \\ & R_{19} y^2 \text{Sinh } \beta y + R_{25} y^2 \text{Cosh } 2\beta y + R_{41} y^2 \text{Sinh } 2\beta y + R_{21} y^3 \text{Cosh } \beta y + R_{42} y^3 \text{Sinh } \beta y \\ & + R_{27} y^3 \text{Sinh } 2\beta y + R_{43} y^4 \text{Cosh } \beta y - R_{23} y^4 \text{Sinh } \beta y + R_{26} y^4 \text{Cosh } 2\beta y + \\ & R_{22} y^5 \text{Cosh } \beta y + R_{20} y^5 \text{Sinh}\beta y + R_{28} + R_{24} y^6 \text{Cosh } \beta y + R_{28} y^5 \text{Sinh } 2\beta y + \\ & R_{29} y^6 \text{Cosh } 2\beta y + R_{44} \text{Sinh } 2\beta y \text{Cosh } \beta y + R_{45} \text{Sinh } \beta y \text{ Cosh } 2\beta y - R_{46} y^6 + R_{17} y^5 + \\ & R_{47} y^4 + R_{48} y^3 + R_{49} y^2 + R_{50} y + R_{51}\end{aligned} \tag{34}$$

The heat transfer coefficient in terms of wall slope parameter ‘δ’ is

$$z = z_0 + \delta z_1 + \ldots\ldots \tag{35}$$

$$z_0 = \left(\frac{\partial \eta}{\partial x}\right)\left(\frac{\partial \theta_0}{\partial y}\right) \tag{36}$$

$$z_1 = \left(\frac{\partial \theta_0}{\partial x}\right) + \left(\frac{\partial \eta}{\partial x}\right)\left(\frac{\partial \theta_1}{\partial y}\right) \tag{37}$$

where

$$A_1 = \delta((M_1 \eta + m_{10} \eta^3) \text{ Cosh}[\beta \eta] + M_2 \eta^2 \text{ Sinh}[\beta \eta] + M_{11} \eta^5 + M_3 \eta^3 + M_4 \eta)$$

$$\begin{aligned}A_2 = {} & \frac{\delta \text{ Sinh}[\beta\eta]}{\beta}((M_5 + m_{16}) + m_{15} \eta^2) \text{ Sech}[\beta \eta] + ((M_7 + m_{17} + m_{20} + m_{21} + M_9)\eta \\ & + m_{14} \eta^3) \text{ Tanh}[\beta\eta] + (m_{11} + m_{14} + M_{10})\eta^2 + (M_6 + m_9 + m_{10} + M_8 + M_{11} + M_{12}))\end{aligned}$$

$$A_3 = \delta\Big(\frac{1}{\beta^3}(m_5\eta^3\beta^2 + 6m_5\eta - 2M_{15}\eta\beta + (m_8 + M_{14} + M_{16})\eta\beta^2)\ \mathrm{Cosh}[\beta\ \eta]$$

$$+\frac{1}{\beta^4}(2M_{15}\beta - (m_8 - M_{14} + M_{16} + 3m_5\eta^2)\beta^2 + M_{15}\eta^2\beta^3 - 6m_5)\mathrm{Sinh}[\beta\eta] +$$

$$\frac{m_{10}}{5}\eta^5 + \frac{M_3}{3}\eta^3\Big)$$

$$A_4 = \delta\Big(\frac{1}{\beta}(m_3\eta\beta + m_{19}\eta)\mathrm{Cosh}[\beta\ \eta] + \big(\frac{1}{\beta}(m_1\mathrm{Tanh}[\beta\eta] + m_7\eta\mathrm{Sinh}[\beta\eta]\mathrm{Tanh}[\beta\eta] + m_6) +$$

$$\frac{1}{3}(3m_{14}\eta^3 + m_{16}\eta^3)\big)$$

$$A_5 = B_1\eta + \frac{1}{\beta}B_3\mathrm{Sinh}[\beta\ \eta] + \eta^3,\ A_6 = \frac{\eta^2}{4}\frac{\partial p_1}{\partial x} - \eta$$

$a_1, a_2, ..., a_{43}, B_1, B_3, ..., B_{10}, g_1, g_2, ..., g_{25}, G_1, G_2, ..., G_7, h_1, h_2, ..., h_{22}, L_1, L_2, ..., L_8,$
$m_1, m_2, ..., m_{21}, M_1, M_2, ..., M_{16}, R_1, R_2, ..., R_{51}$
are constants.

5. RESULTS AND DISCUSSION

In this analysis we investigate the effect of various governing parameters R, δ, ε, α, γ, p_r and S, on Heat transfer in the fluid phase and the particle phase.

Figs.(1-7) represent heat transfer coefficient z characteristics in fluid phase. Fig.(1) represents the variation of heat transfer z with Reynolds number R, we find that an increase in the Reynolds number R leads to a depreciation in the heat transfer coefficient z. The depreciation in z with R increases with increase in R. The variation of z with Ratio of specific heats γ, reveals that the depreciation in z is very marginal with the increase in γ in the flow region Fig.(2). In Fig.(3) we find that an increase in Dust concentration parameter α reduces z in entire flow region, the depreciation in z with α is almost negligible on the central line y = 0 and it is appreciable as we move towards the boundary y = 1. The variation of z with Prandtl number p_r shows that the heat transfer coefficient experiences a depreciation with p_r , the depreciation on the boundary at y = 1 is appreciably large in Fig(4). The effect of amplitude ratio ε on the coefficient of Heat transfer is shown in Fig.(5).The variation in z with different ε is almost linear as we move from the central line y = 0 to the boundary y =1,the heat transfer coefficient z experiences with ε in the entire flow region. The effect of slope parameter δ on z is exhibited in Fig.(6). The profiles of z with δ shows that the value of z gradually reduces as we move from the central line y = 0 to y = 1.0. An increase in δ leads to an enhancement in z. fig.(6.7) represent the variation of z with S, we find that the values S ≤ 2 the heat transfer coefficient z reduces as we move from the central line to the boundary, while for S ≥ 3, it enhances enhancement with Couple stress parameter S.

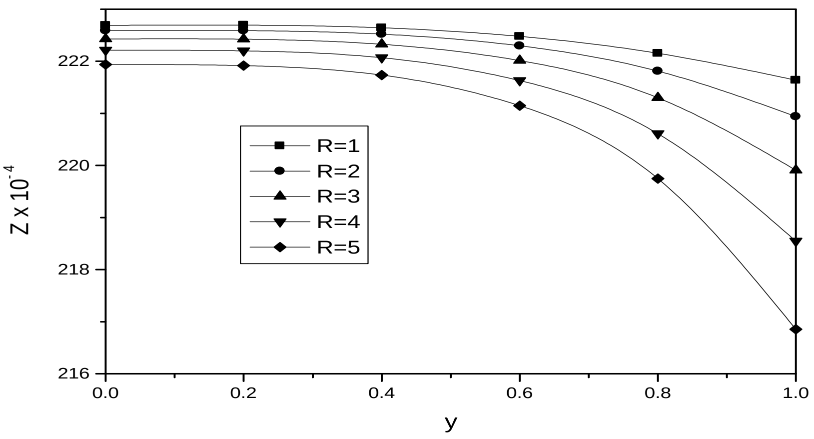

Fig.1-Effect of the Reynolds number R on Z for
$\gamma = 1$, $\alpha = 1$, $\varepsilon = 0.01$, $\delta = 0.01$, , $S = 1$, $P_r = 1$

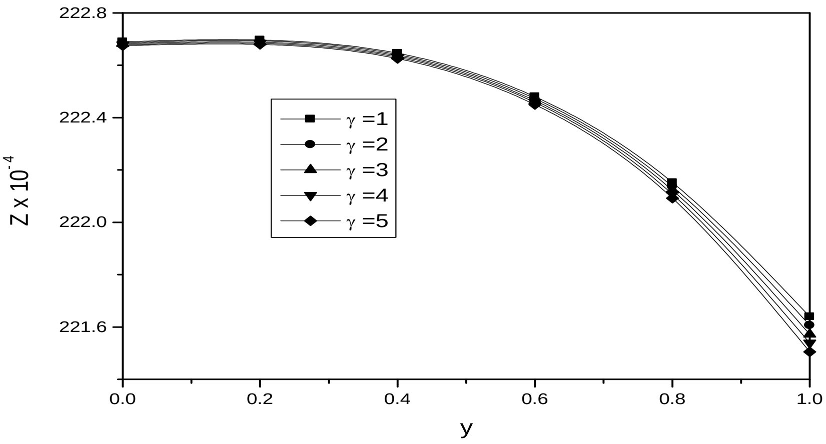

Fig.2-Effect of the Coefficient of Specific heats γon Z for
$R = 1$, $\alpha = 1$, $\varepsilon = 0.01$, $\delta = 0.01$, $S = 1$, $P_r = 1$

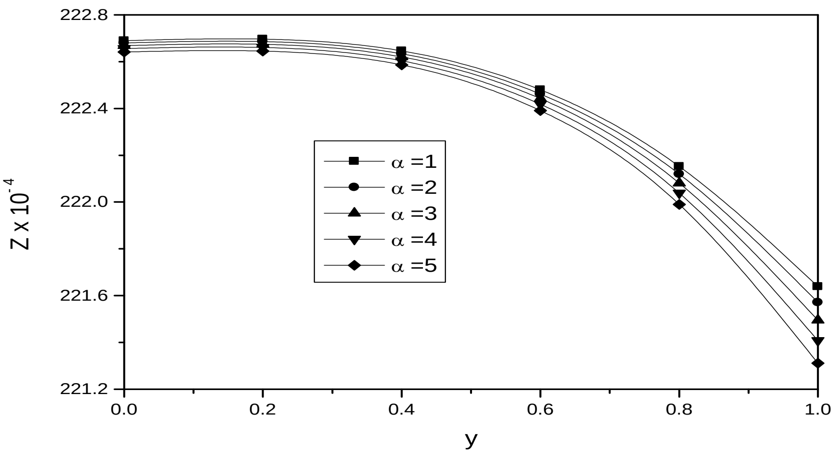

Fig.3- Effect of the Dust Concentration parameter αon Z for
$R = 1$, $\gamma = 1$, $\varepsilon = 0.01$, $\delta = 0.01$, $S = 1$, $P_r = 1$

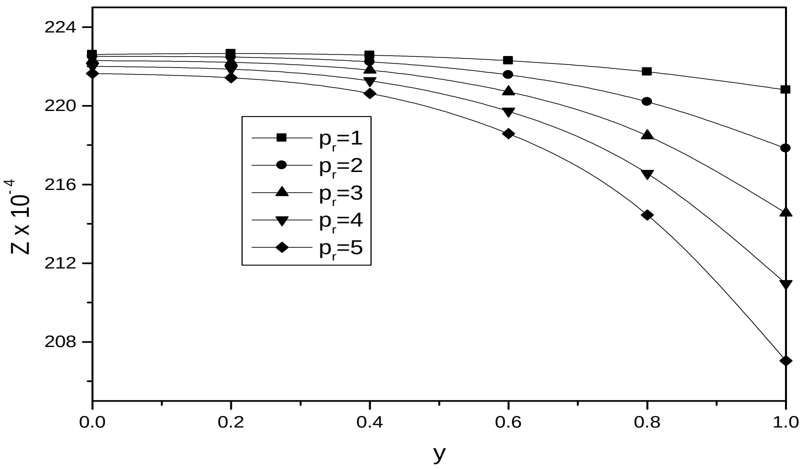

Fig.4- Effect of Prandtl number p_r on Z for
R = 1, γ = 1, ε = 0.01, δ= 0.01, S =1, α = 1

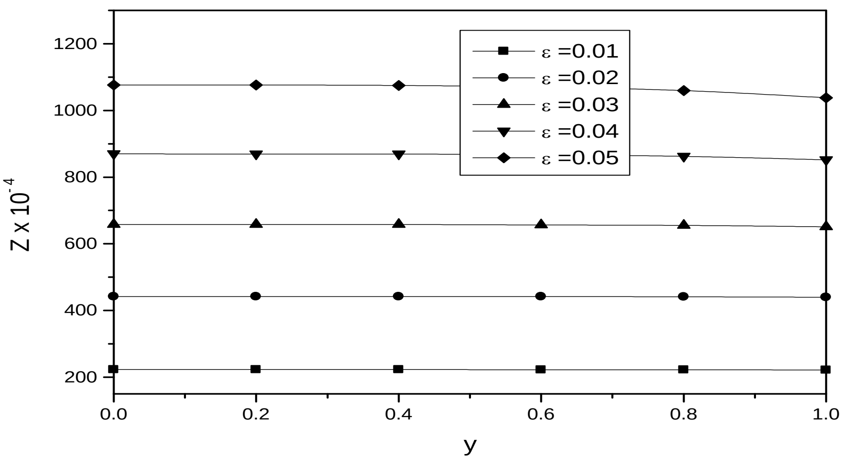

Fig.5- Effect of amplitude ratio ε on Z for
R = 1, γ = 1, P_r = 1, δ= 0.01, S =1, α = 1

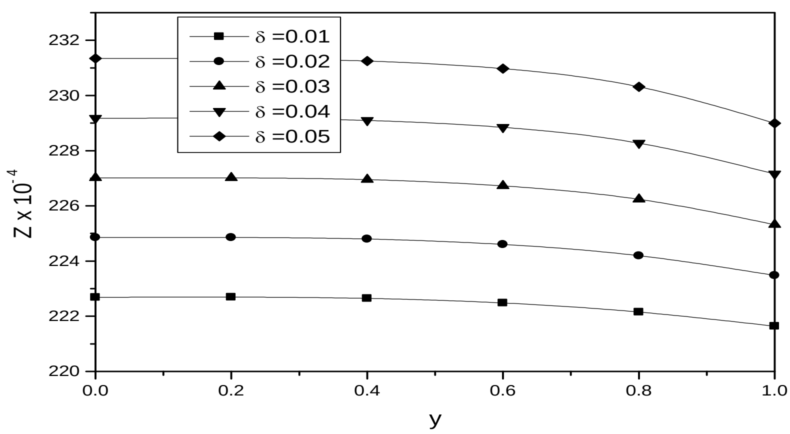

Fig.6- effect of slope parameter δ on Z for
R = 1, γ = 1, P_r = 1, ε= 0.01, S =1, α = 1

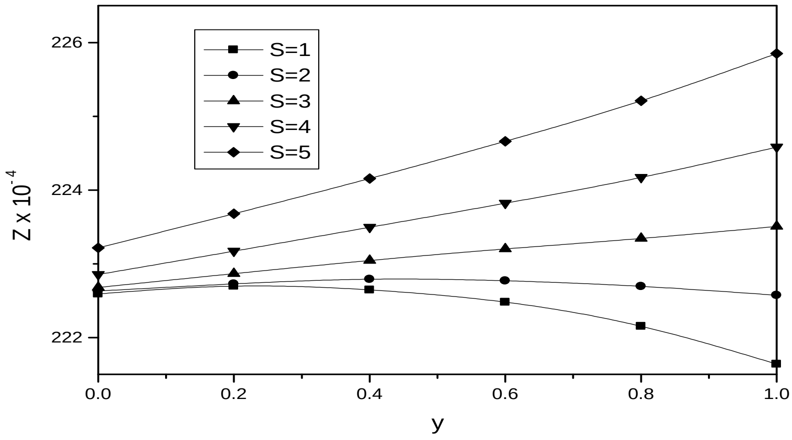

Fig.7- Effect of Couple stress parameter S on Z for
R = 1, γ = 1, P_r = 1, δ= 0.01, δ= 0.01, α = 1

From Figs. (8-14) represents the variation of heat transfer coefficient z* with R,δ, ε, α, γ, p_r and S in the particle phase. From figs (8-14) we find that the heat transfer coefficient z* in the particle phase reduces gradually as we move from the central line y = 0 to boundary y = 1. An increase in the Reynolds number R results in a depreciation in z*.Fig(8)The depreciation in z* with R is marginal at the central line y = 0 and is appreciably large at y = 1. Fig.(9)The variation of transfer coefficient z* with Ratio of specific heats γ reveals that z* experiences marginal enhancement with increase in γ. From Fig.(10) the variation of z*with Dust concentration parameter α shows that the depreciation in z* is marginal in the central line and appreciable at y = 0. From Fig.(11) the variation of heat transfer coefficient z* with Prandtl number P_r , we find that as we move from central line y = 0 to y =1 heat transfer coefficient z* gradually reduces and it depreciates with increase in P_r. Fig.(12) the variation of z* with amplitude ratio ε, shows that z* is almost linear with any value of ε, as we move from y = 0 to y = 1,also it experiences an enhancement with increase in ε. Fig.(13) represent the variation of z* with slope parameter δ, it is found that higher the slope δ of the boundary layer the heat transfer coefficient z*. Fig.(14) The variation of heat transfer coefficient z* with couple stress parameter S shows that for S $\leq$ 2, z* decreases gradually from y = 0 to y =1 and for higher S $\geq$ 3, it enhances as we move the central line to the boundary also higher the couple stress parameter S larger the heat transfer coefficient z*.

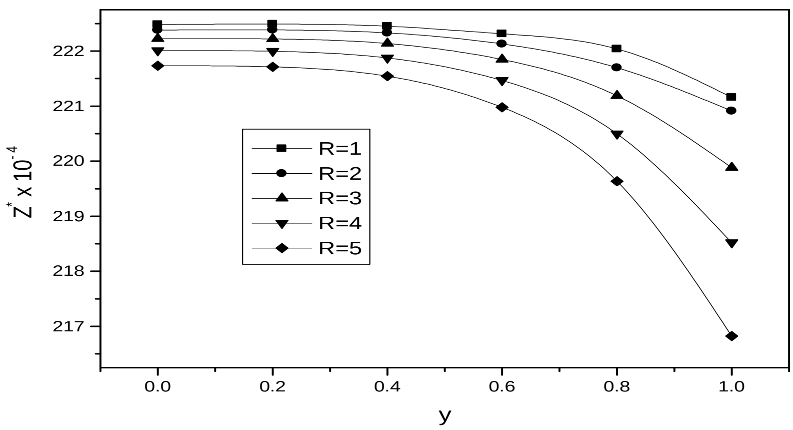

Fig.8-Effect of the Reynolds number R on z* for
γ = 1, α = 1, ε = 0.01, δ= 0.01, , S =1, P_r = 1

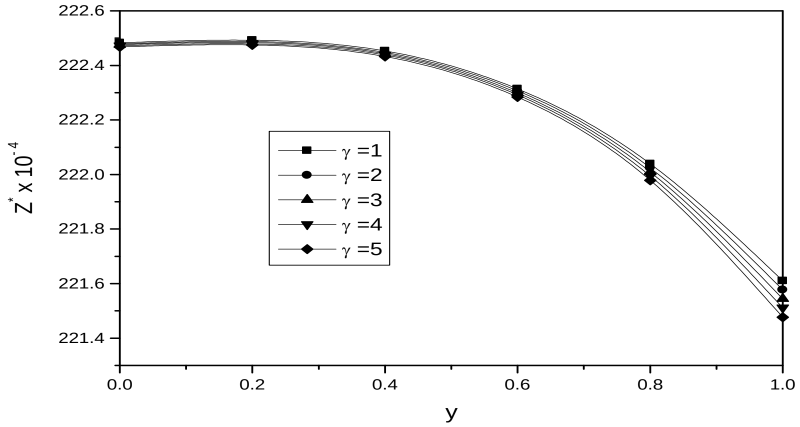

Fig.9-Effect of the Coefficient of Specific heats γon z* for
R = 1, α = 1, ε = 0.01, δ= 0.01, S =1, P_r = 1

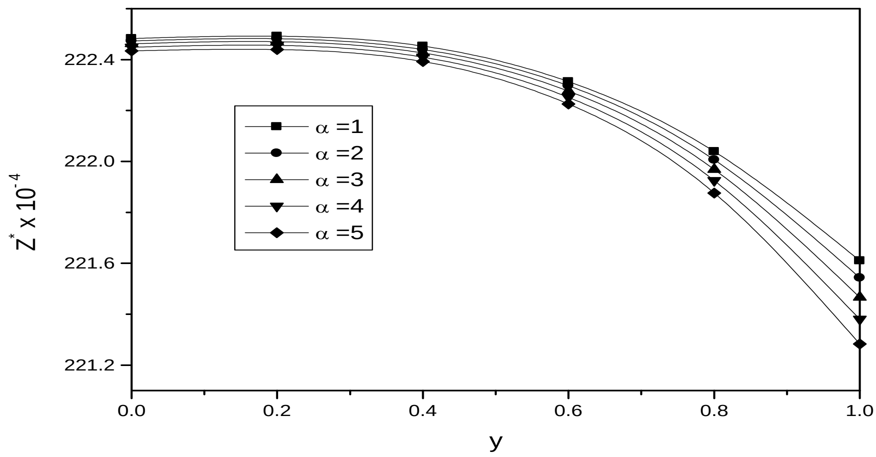

Fig.10- Effect of the Dust Concentration parameter αon z* for
R = 1, γ = 1, ε = 0.01, δ= 0.01, S =1, P_r = 1

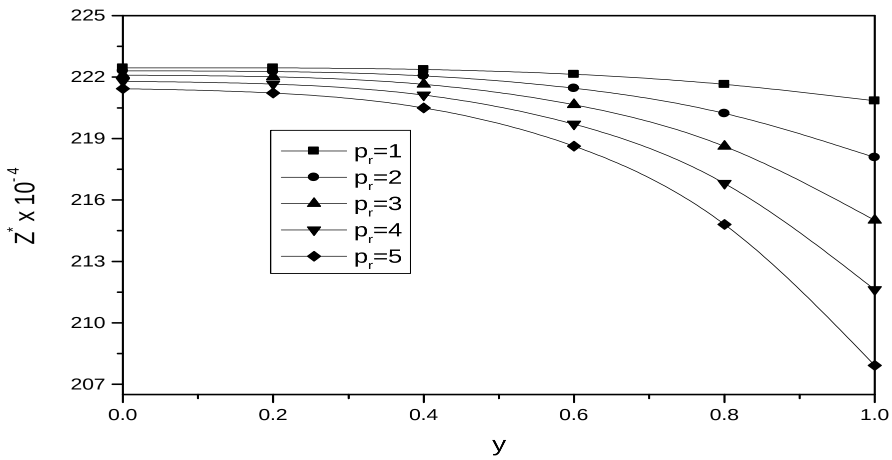

Fig.11- Effect of Prandtl number p_r on z* for
R = 1, γ = 1, ε = 0.01, δ= 0.01, S =1, α = 1

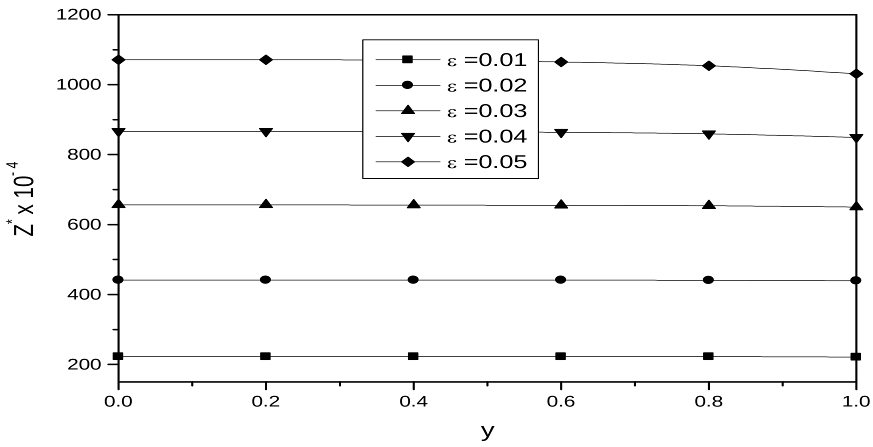

Fig.12- Effect of amplitude ratio ε on z* for
R = 1, γ = 1, P_r = 1, δ= 0.01, S =1, α = 1

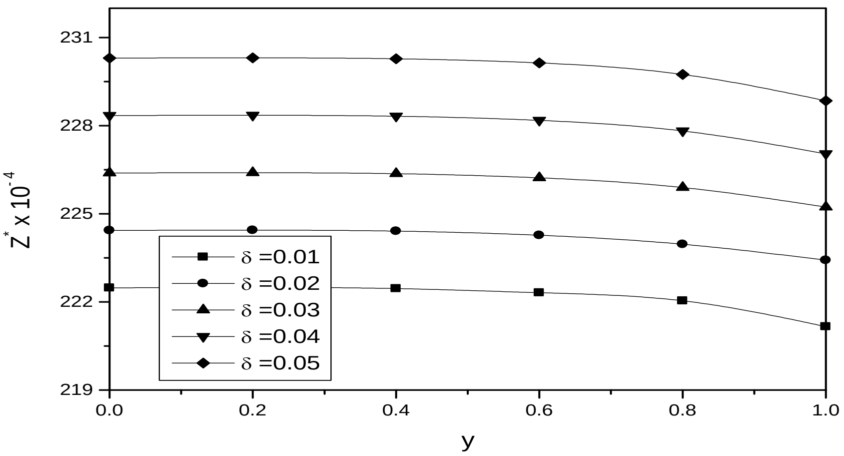

Fig.13-effect of slope parameter δ on z* for
R = 1, γ = 1, P_r = 1, ε= 0.01, S =1, α = 1

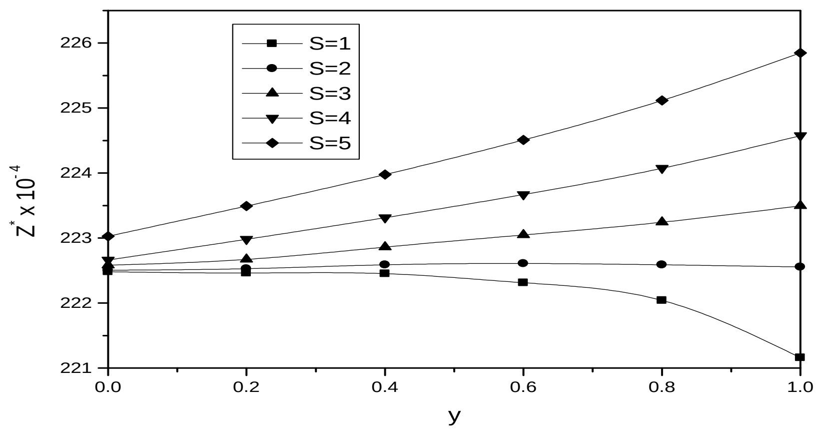

Fig.14- Effect of Couple stress parameter S on z* for
R = 1, γ = 1, P_r = 1, δ= 0.01, δ= 0.01, α = 1

6. CONCLUSION

In conclusion, this study highlights the significant impact of heat transfer on the peristaltic transport of particle-suspended couple stress fluids. The results demonstrate that the Prandtl number and couple stress parameters notably influence the heat transfer behavior, with an observed decrease in heat transfer efficiency as the Prandtl number increases. Additionally, the boundary effects at y = 1 show considerable changes in the heat transfer coefficient. These findings provide valuable insights for optimizing systems involving peristaltic flows, such as biomedical devices and microfluidic applications, where efficient thermal management is essential. Further research could explore the effects of varying fluid properties, such as viscosity and thermal conductivity, in more complex geometries or under different flow regimes. Expanding the study to include more realistic particle behaviors, such as size distribution and aggregation, could also enhance the applicability of the results to real-world scenarios in biofluid transport and microfluidic devices.

7. REFERENCES

1. Vidhya, M., Siva, E. P., & Govindarajan, A. (2015). Peristaltic flow of couple-stress fluid with heat and mass transfer: An application in biomedicine. *ResearchGate*. https://www.researchgate.net/publication/276509791_Peristaltic_flow_of_couple-stress_fluid_with_heat_and_mass_transfer_An_application_in_biomedicine
2. Prasad, K. M., Subadra, N., & Mahabaleshwar, U. S. (2017). Peristaltic transport of couple-stress fluid carrying nanoparticles: Heat and mass transfer effects. *International Journal of Engineering and Technology*, 48(2), 262-270. https://ijettjournal.org/archive/ijett-v48p262
3. Naga Charan Nandigama. (2020). An integrated data engineering and data science architecture for scalable analytical warehousing and real-time decision systems. International Journal of Business Analytics and Research (IJBAR), Nov 2020, 10(1), 20-26.
4. Ramesh, K., & Devakar, M. (2015). Heat transfer in magnetohydrodynamic peristaltic flow of couple-stress fluids. *Mathematical Problems in Engineering*, 2015, 1-10. https://doi.org/10.1155/2015/163832
5. Maiti, S., & Misra, J. C. (2012). Peristaltic transport of couple-stress fluids in a porous medium: Effects of particle suspension. *Journal of Biomechanics*, 45(5), 889-895. https://doi.org/10.1016/j.jbiomech.2012.01.005
6. N. C. Nandigama, "Data-Warehouse-Enhanced Machine Learning Framework for Multi-Perspective Fraud Detection in Multi-Stakeholder E-Commerce Transactions," International Journal on Recent and Innovation Trends in Computing and Communication, vol. 11, no. 5, pp. 592–600, May 2023, doi: 10.17762/ijritcc.v11i5.11808.
7. Bhatti, M. M., & Ellahi, R. (2021). Heat transfer in particle-suspended couple-stress fluid flow with nanoparticles in peristaltic transport. *Mathematical and Computational Applications*, 26(2), 36. https://doi.org/10.3390/mca26020036
8. Ahmed, S., Zahra, W., & Ullah, I. (2016). Hemodynamics of blood flow in a couple-stress fluid model with heat transfer. *Computational and Mathematical Methods in Medicine*, 2016, 2016. https://doi.org/10.1155/2016/4029615
9. Ghosh, S., & Roy, S. (2017). Fluid-particle interactions in microfluidic peristaltic channels: Effects of heat and mass transfer. *International Journal of Heat and Mass Transfer*, 111, 321-328. https://doi.org/10.1016/j.ijheatmasstransfer.2017.03.014

10. Raju, B. M., Yadav, K., & Sharma, S. (2019). Effect of suspended particle concentration on heat transfer in peristaltic transport systems. *Journal of Thermal Science and Engineering Applications*, 11(4), 041004. https://doi.org/10.1115/1.4043185